Microbiology (2005), **151**, 1083–1094 DOI 10.1099/mic.0.27667-0

Elucidation of stability determinants of cold-adapted monomeric isocitrate dehydrogenase from a psychrophilic bacterium, *Colwellia maris*, by construction of chimeric enzymes

Seiya Watanabe,†‡ Yoshiaki Yasutake,‡ Isao Tanaka and Yasuhiro Takada

Division of Biological Sciences, Graduate School of Science, Hokkaido University, Sapporo, Hokkaido 060-0810, Japan

Correspondence
Yasuhiro Takada
ytaka@sci.hokudai.ac.jp

Received 30 September 2004
Revised 6 December 2004
Accepted 15 December 2004

To elucidate determinants of differences in thermostability between mesophilic and psychrophilic monomeric isocitrate dehydrogenases (IDHs) from *Azotobacter vinelandii* (*Av*IDH) and *Colwellia maris* (*Cm*IDH), respectively, chimeric enzymes derived from the two IDHs were constructed based on the recently resolved three-dimensional structure of *Av*IDH, and several characteristics of the two wild-type and six chimeric IDHs were examined. These characteristics were then compared with those of dimeric IDH from *Escherichia coli* (*Ec*IDH). All recombinant enzymes with a $(His)_6$-tag attached to the N-terminal were overexpressed in the *E. coli* cells and purified by Ni^{2+}-affinity chromatography. The catalytic activity (k_{cat}) and catalytic efficiency (k_{cat}/K_m) of the wild-type *Av*IDH and *Cm*IDH were higher than those of *Ec*IDH, implying that an improved catalytic rate more than compensates for the loss of a catalytic site in the former two IDHs due to monomerization. Analyses of the thermostability and kinetic parameters of the chimeric enzymes indicated that region 2, corresponding to domain II, and particularly region 3 located in the C-terminal part of domain I, are involved in the thermolability of *Cm*IDH, and that the corresponding two regions of *Av*IDH are important for exhibiting higher catalytic activity and affinity for isocitrate than *Cm*IDH. The relationships between the stability, catalytic activity and structural characteristics of *Av*IDH and *Cm*IDH are discussed.

INTRODUCTION

$NAD(P)^+$-dependent isocitrate dehydrogenase [IDH, EC 1.1.1.41(42)] occupies a key position in the TCA cycle and catalyses a reaction consisting of dehydrogenation and concomitant decarboxylation, as follows:

$$\text{isocitrate} + \text{NAD(P)}^+ \leftrightarrow \text{2-oxoglutarate} + \text{CO}_2 + \text{NAD(P)H}$$

The catalytic mechanism and structure of IDH have been studied most extensively in *Escherichia coli* (*Ec*IDH). From these studies, it has been clarified that *Ec*IDH binds to a coenzyme by using a unique motif, other than the Rossmann fold shared by many $NAD(P)^+$-dependent dehydrogenases (Chen & Jeong, 2000). $NADP^+$-IDHs of many bacteria, including *E. coli*, are known to be homodimers of subunits of about 40–45 kDa, although a monomeric IDH with a molecular mass of about 80–100 kDa is also found in eubacteria. Bacteria generally possess only one type of IDH. The monomeric and dimeric IDHs differ in amino acid sequence and immunological cross-reactivity (Ishii *et al.*, 1993; Eikmanns *et al.*, 1995; Sahara *et al.*, 2002). The dimeric *Ec*IDH and a monomeric IDH from *Azotobacter vinelandii* show only a 7–8 % identity in amino acid sequence alignment, based on their structures. This implies that the monomeric and dimeric IDHs have evolved convergently.

A psychrophilic bacterium, *Colwellia maris* (Takada *et al.*, 1979; Yumoto *et al.*, 1998), has both monomeric and dimeric IDHs (Ochiai *et al.*, 1979). Its monomeric IDH (*Cm*IDH) exhibits maximal activity at 20 °C, and even at 30 °C is rapidly inactivated, indicating that it is a typical cold-adapted enzyme. Such psychrophilic enzymes are one of the mechanisms for biological adaptation to permanently cold environments and have two common

†Present address: Institute of Advanced Energy, Kyoto University, Gokasho, Uji, Kyoto 611-0011, Japan.

‡These authors contributed equally to this work.

Abbreviations: CD, circular dichroism; IDH, isocitrate dehydrogenase; IPMDH, isopropylmalate dehydrogenase; MALDI-TOF, matrix-assisted laser desorption/ionization time-of-flight; $t_{½}$, half-life.

characteristics: high catalytic activity at low temperatures and low thermostability compared to mesophilic and thermophilic counterparts (Gerday *et al.*, 1997). These characteristics are considered to be closely related to each other, because the enhanced conformational flexibility of the enzyme proteins responsible for the thermolability may be necessary to accommodate the substrates, the diffusion rates of which are inevitably diminished at low temperatures, and to bring about rapid conformational changes for the catalysis without energy loss (Fields & Somero, 1998). Recent structural comparisons of homologous enzyme proteins from psychrophilic, mesophilic and thermophilic organisms indicate that there may be numerous structural features of psychrophilic enzymes responsible for increased thermolability (Fields & Somero, 1998; Russell *et al.*, 1998; Alvarez *et al.*, 1998; Kim *et al.*, 1999; Bentahir *et al.*, 2000; de Backer *et al.*, 2002).

The monomeric IDH of a mesophilic nitrogen-fixing bacterium, *Azotobacter vinelandii*, (*Av*IDH) showed 66 % identity and 78 % similarity in amino acid sequence to *Cm*IDH (Ishii *et al.*, 1993; Sahara *et al.*, 2002), indicating that their tertiary structures are similar to each other. However, the former was found to be a typical mesophilic enzyme (optimal temperature for activity, 40–45 °C), and the two IDHs differed in thermostability and optimal temperature for activity. On the other hand, the three-dimensional structure and active site of *Av*IDH recently resolved by crystallographic analysis (Yasutake *et al.*, 2002, 2003) allow us to analyse the relationship between the temperature-dependent characteristics and structure of enzymes. Therefore, based on the three-dimensional structure of *Av*IDH, we constructed chimeric enzymes, in which various combinations of three regions of *Av*IDH and *Cm*IDH were fused, and examined their temperature-dependent characteristics for catalytic function and structural stability.

The dimeric *Ec*IDH has two catalytic sites, which are located at the interfaces of the two identical subunits and are formed by amino acid residues derived from both subunits (Hurley *et al.*, 1989, 1991). On the other hand, the crystal structure of the monomeric *Av*IDH (Yasutake *et al.*, 2002) reveals that this enzyme contains domain I, consisting of N- and C-terminal segments (regions 1 and 3, respectively), and domain II, corresponding to the intermediate segment (region 2), and that the single polypeptide chain acquires the ability to catalyse a reaction identical to the dimeric IDH by fusing domain B′–C′ of the second subunit to the first subunit with the same spatial relationship (Fig. 1). This suggests that monomeric IDH may have evolved through the duplication of domain B–C in an ancestral dimeric IDH, rather than convergently. Although monomeric *Cm*IDH and *Av*IDH and dimeric *Ec*IDH catalyse the same reaction, and exhibit the same specificity for the coenzyme ($NADP^+$) and metal ion (Mn^{2+} or Mg^{2+}), the former two IDHs can be considered to have lost one catalytic site by the monomerization. Accordingly, in this paper, we also compared the catalytic properties of monomeric and dimeric bacterial IDHs.

METHODS

Construction of genes encoding chimeras between *Cm*IDH and *Av*IDH. The *icd* genes encoding *Av*IDH, *Cm*IDH and *Ec*IDH were amplified by PCR to introduce restriction sites for *Bam*HI and *Sac*I at the 5′- and 3′-terminals of the ORFs, respectively. Therefore, the following primers were synthesized: for *Av*IDH, *AF0* 5′-gcgcggatccgTCCACACCGAAGATTATC-3′ (29-mer) and *AR0* 5′-gcgcgagctcTTATGCAAGAGGTGCCAG-3′ (28-mer); for *Cm*IDH, *CF0* 5′-gcgcggatccgAGCACTGATAACTCAAAAATC-3′ (32-mer) and *CR0* 5′-gcgcgagctcTTAAAGTAATGCAGATAAAATGG-3′ (33-mer); for *Ec*IDH, *EcF* 5′-gcgcggatccgGAAAGTAAAGTAGTTG-3′ (27-mer) and *EcR* 5′-gcgcgagctcTTACATGTTTTCGATGATC-3′ (29-mer) [lower-case type indicates additional bases for introducing digestion sites for *Sac*I and *Bam*HI (underlined)]. PCR was carried out in a DNA thermal cycler 2400 (Perkin-Elmer) in a 50 µl reaction mixture containing about 10 pmol of each primer, 1 U KOD-plus DNA polymerase (Toyobo) and 100 ng pAVESc (Sahara *et al.*, 2002), pIS202 (Ishii *et al.*, 1993) or pTK512 (Thorsness & Koshland, 1987) carrying the *icd* genes of *A. vinelandii*, *C. maris* and *E. coli*, respectively, as template DNA in a buffer system prepared by the manufacturer. Cycling conditions were as follows: denaturation at 94 °C for 15 s, annealing at 50 °C for 30 s, and extension at 68 °C for time periods calculated based on an extension rate of 1 kbp min^{-1}. Each amplified PCR fragment was ligated to the *Bam*HI–*Sac*I site of pTrcHisB (Invitrogen), a plasmid vector for conferring the N-terminal $(His)_6$-tag on the expressed proteins, to obtain the plasmids pHis*AvWT*, pHis*CmWT* and pHis*EcWT*, respectively.

The *icd* gene of *Av*IDH possesses *Bss*HII and *Nsp*V sites between regions 1 and 2 and between regions 2 and 3, respectively (Fig. 1e), but a *Bss*HII site is absent in the corresponding region of the *C. maris icd* gene. Therefore, to exchange each domain of *Av*IDH and *Cm*IDH, a *Bss*HII site was introduced into the *icd* of *C. maris* by PCR, as described above. For this reaction, the following two primers were used: *C.m.BssHII-s* 5′-GGTAACTCTGATCGTCGcGCGCCAGCG-3′ (27-mer) and *C.m.BssHII-as* 5′-CGCTGGCGCgCGACGATCAGAG-TTACC-3′ (27-mer) [lower-case type indicates bases substituted to introduce the *Bss*HII site (underlined)]. Two PCR products were obtained in separate reactions with the primer sets *CF0* plus *C.m.BssHII-as* and then *C.m.BssHII-s* plus *CR0*. The products were used as template DNAs for a third PCR reaction with the primers *CF0* and *CR0*. The resultant PCR product was digested with *Bam*HI and *Sac*I, and was then ligated to the *Bam*HI–*Sac*I site of pTrcHisB to obtain the plasmid pHis*Cm-Bss*HII. The introduction of the *Bss*HII site in *Cm*IDH resulted in no change of amino acid residues, because the codon of Arg116, CGT, was replaced by another codon for Arg, CGC. After the *A. vinelandii* and *C. maris icd* genes had been amplified by PCR with pHis*AvWT* and pHis*Cm-Bss*HII as template DNA and the primer sets *AF0* plus *AR0* and *CF0* plus *CR0*, respectively, the resulting products were digested with *Bss*HII and *Nsp*V to obtain six DNA fragments corresponding to regions 1 to 3 of *Av*IDH and *Cm*IDH (fragments 1_{Av}–3_{Av} and 1_{Cm}–3_{Cm}, respectively). Fragments 1_{Av}, 2_{Cm} and 3_{Av} and fragments 1_{Cm}, 2_{Av} and 3_{Cm} were ligated to the *Bam*HI–*Sac*I site of pTrcHisB to obtain the plasmids pHis*ACA* and pHis*CAC*, respectively. Similarly, for the exchange of region 1 of the two enzymes, four DNA fragments produced by the digestion of the amplified *Av*IDH and *Cm*IDH ORFs with *Bss*HII were ligated with combinations of fragments 1_{Cm} and 2–3_{Av} and fragments 1_{Av} and 2–3_{Cm} to obtain pHis*CAA* and pHis*ACC*, respectively. To construct chimeric IDHs with replacements of region 3, the *Nsp*V site in the vector pTrcHisB located downstream of the inserted *icd* gene was utilized. The *Nsp*V fragments of pHis*CmWT* and pHis*AvWT* were

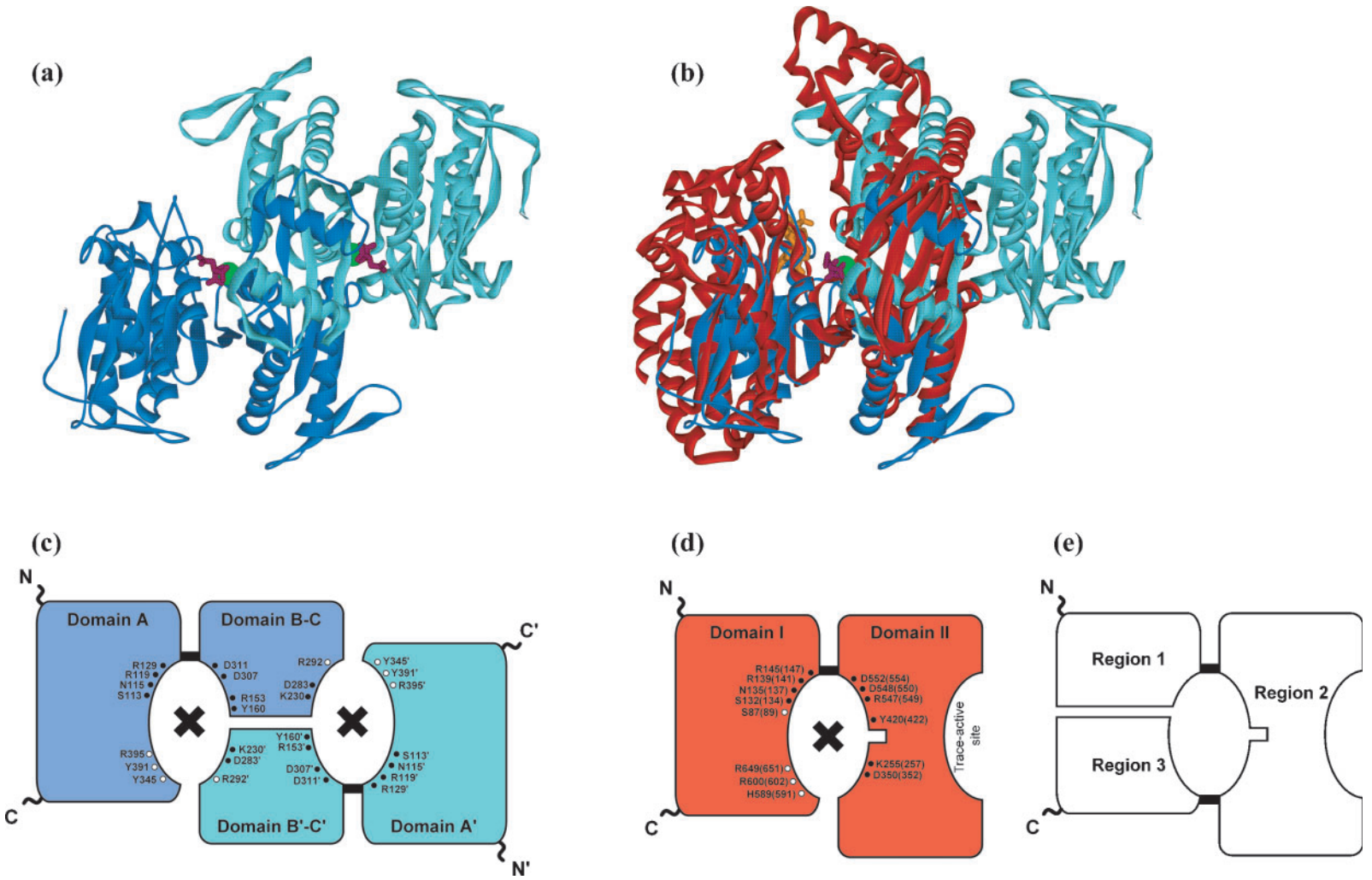

Fig. 1. Structure of dimeric and monomeric IDHs. (a) Ribbon model of dimeric *Ec*IDH. Two identical (first and second) subunits are coloured in blue and light blue, respectively. Isocitrate and Mg^{2+} bound to catalytic sites are shown by violet sticks and green spheres, respectively. (b) Ribbon model of monomeric *Av*IDH (red) superimposed onto (a). Isocitrate, Mg^{2+} and $NADP^{+}$ are depicted as in (a). (c) and (d) Respective schematic representations of the catalytic sites of dimeric *Ec*IDH and monomeric *Av*IDH. The colour of each region is the same as in (a) and (b). Closed and open circles indicate amino acid residues bound to isocitrate plus Mn^{2+} (or Mg^{2+}) and $NADP^{+}$, respectively. Crosses represent the catalytic sites. N and C show each terminal of the protein. In *Ec*IDH, the second subunit and its amino acid residues are prime-signed. In (d), numbers in parentheses show the positions of the corresponding amino acid residues in *Cm*IDH. (e) Schematic representation of each region in monomeric IDH.

exchanged and ligated to yield the plasmids pHis*CCA* and pHis*AAC*. The coding regions of these chimeric genes were confirmed by subsequent DNA sequencing in both directions.

Overexpression and purification of His-tagged IDHs. Cells of an *E. coli* mutant defective in IDH, DEK2004 (Thorsness & Koshland, 1987; LaPorte *et al.*, 1985), harbouring the expression plasmid for the His-tagged wild-type *Av*IDH, *Cm*IDH and *Ec*IDH (*Av*WT, *Cm*WT and *Ec*WT, respectively) and chimeric IDHs (*AAC*, *ACA*, *CAA*, *CCA*, *CAC* and *ACC*) were grown at 37 °C to a turbidity of 0·6 at 600 nm in Super broth medium (12 g tryptone, 24 g yeast extract, 5 ml glycerol, 3·81 g KH_2PO_4 and 12·5 g K_2HPO_4 l^{-1}, pH 7·0) containing 50 mg ampicillin l^{-1} and 15 mg tetracycline l^{-1}. The cultures were then rapidly cooled on ice and further incubated for 18–24 h at 15 °C after the addition of 1 mM IPTG to induce the expression of the IDH protein. The inductions of gene expression by IPTG were carried out at low temperatures, such as 15 °C, because of the marked thermolability of *Cm*IDH (Ochiai *et al.*, 1979). Cells were harvested and resuspended in 20 ml Buffer A (50 mM sodium phosphate, pH 8·0, containing 2 mM $MgCl_2$, 0·5 M NaCl, 10 mM 2-mercaptoethanol and 10 mM imidazole) per litre of the culture. Hen-egg lysozyme was added to the cell suspension at a concentration of 2 mg ml^{-1} and the mixture was gently shaken overnight at 4 °C. The cells were then disrupted by ultrasonic oscillation. After the centrifugation of the cell lysate at 39 120 ***g*** for 30 min at 4 °C to remove cell debris, the supernatant was centrifuged at 105 000 ***g*** for 6 h at 4 °C. The resultant supernatant was loaded onto a Ni-NTA column (25 ml, Qiagen) equilibrated with Buffer A. After a thorough washing with the same buffer, the column was further washed with 50 ml Buffer B (Buffer A containing 10 %, v/v, glycerol and 20 mM imidazole instead of 10 mM imidazole) and next with 50 ml Buffer C (Buffer B containing 30 mM instead of 20 mM imidazole). The enzymes were then eluted with 50 ml Buffer D (Buffer B containing 250 mM instead of 20 mM imidazole). The elutant was concentrated with PEG 20 000 and dialysed against Buffer E (20 mM sodium phosphate, pH 8·0, containing 2 mM $MgCl_2$, 0·5 M NaCl, 0·05 mM sodium citrate, 1 mM DTT and 50 %, v/v, glycerol). All His-tagged recombinant IDHs were stored at −35 °C until use.

Enzyme assay. The IDH activity was assayed as described previously (Ochiai *et al.*, 1979). For *Av*WT, *ACA*, *CCA*, *CAA* and *Ec*WT, 0·25 M NaCl was omitted from the reaction mixture. In the heat-inactivation experiment, all purified recombinant IDHs were dialysed overnight at 4 °C against 20 mM potassium phosphate buffer (pH 8·0) containing 2 mM $MgCl_2$, 0·1 M NaCl, 10 % (v/v) glycerol and 1 mM DTT (Buffer F). After incubation for 10 min at various temperatures, the enzymes were withdrawn and immediately cooled on ice for 10 min. The residual activity was then assayed at the optimal temperature for activity of each enzyme. Protein concentration was determined by the method of Lowry *et al.* (1951) with BSA as standard.

SDS-PAGE and Western blot analysis. SDS-PAGE was carried out by the method of Laemmli (1970) with 10 % or 15 % gel at 25 mV. After SDS-PAGE of the purified IDHs, the proteins on the gels were transferred onto a nitrocellulose membrane (Hybond-C, Amersham Pharmacia Biotech). Western blot analysis was performed with the ECL Western blotting detection system (Amersham Pharmacia Biotech) and either rabbit polyclonal antibodies against the monomeric IDH from *Vibrio parahaemolyticus* (Fukunaga *et al.*, 1992) or the *C. maris* dimeric IDH isozyme I (Ishii *et al.*, 1987), or mouse monoclonal antibody against the $(His)_6$-Gly in the N-terminal His-tag of the expressed recombinant proteins (Invitrogen). Native *Av*IDH was purified as described previously (Yasutake *et al.*, 2001).

Circular dichroism (CD). Enzyme samples dialysed overnight against Buffer F were diluted to a concentration of 0·5 mg protein ml^{-1} with the same buffer. CD measurements at 220 nm were carried out between 10 °C and 70 °C with a Jasco spectropolarimeter model J-720 by using a cuvette with a path length of 1 mm. Temperature was increased at a rate of 1 °C min^{-1}.

Digestion with trypsin. The purified recombinant IDHs were dialysed overnight at 4 °C against 0·1 M $NaHCO_3$, pH 8·1. The enzyme samples (1 mg ml^{-1}) were incubated for various times at 25 °C with trypsin (0·01 mg ml^{-1}). The proteolysis was stopped by the addition of an equal volume of 2× SDS-PAGE sample buffer. The mixtures were immediately boiled and analysed by SDS-PAGE.

Amino acid sequencing and matrix-assisted laser desorption/ionization time-of-flight (MALDI-TOF) mass spectrometry. After SDS-PAGE of *Cm*WT, *ACA*, *CAC*, *AAC*, *CCA* and *ACC* digested for 30 min with trypsin under the conditions described above, the gels including 58–62 kDa peptide fragments were cut off and broken in 20 mM Tris/HCl (pH 8·0) containing 1 % (w/v) SDS. The peptide fragments were extracted from the gels by vigorous mixing overnight. A fourfold volume of acetone chilled at −20 °C was then added to the extracts. After cooling for 1 h at −80 °C, the mixture was centrifuged at 39 120 ***g*** for 15 min at 4 °C. The precipitates were then dried and dissolved in a small volume of 0·1 % (w/v) SDS. The solutions were coated onto a PVDF membrane (Hybond-P, Amersham Pharmacia Biotech). N-terminal amino acid sequences of the peptide fragments were confirmed by automated Edman degradation on a Hewlett Packard protein sequencer G1005A to clarify the digestive site with trypsin. To determine the C-terminal structure of the proteolytic intermediate from *Cm*WT, the peptides precipitated by acetone were digested at room temperature with carboxypeptidase Y (Oriental Yeast) in 50 µl of 100 mM potassium phosphate (pH 5·6) containing 0·1 % (w/v) SDS and 0·1 mM DL-norleucine (as a standard amino acid) at an enzyme : substrate ratio of 1 : 100. After digestion for various times between 0 and 20 min, 5 µl of the reaction mixture was withdrawn and mixed with an equal volume of 20 % (v/v) acetic acid. The liberated amino acids were determined by a JEOL AminoTac JLC-500/V automatic amino acid analyser. The molecular mass of the proteolytic intermediates from *Cm*WT in 0·1 % (w/v) SDS solution was determined using a MALDI-TOF mass spectrometer (Voyager DE Pro, PE biosystems).

RESULTS

Overexpression and purification of wild-type and chimeric IDHs

As shown in Fig. 2a, SDS-PAGE analysis revealed that the purities of the recombinant enzymes with His-tags at the N-terminal were at least 90–95 %, and the apparent molecular masses of the monomeric IDHs (*Av*WT and *Cm*WT and their chimeric IDHs) and dimeric *Ec*WT were 80 kDa and 43 kDa, respectively, similar to those of the respective native enzymes (Sahara *et al.*, 2002; Thorsness & Koshland, 1987; Ishii *et al.*, 1987). All the purified recombinant IDHs were able to cross-react with antibody against His-tag (Fig. 2c), but no cross-reactivity with antibody against monomeric IDH was observed in *Ec*WT (Fig. 2b), as reported previously (Fukunaga *et al.*, 1992).

Optimal temperature for activity and thermostability

The effect of temperature on the activities of wild-type and chimeric IDHs was examined (Fig. 3a). The optimal temperatures for activity (T_{opt}) of *Av*WT and *Cm*WT with

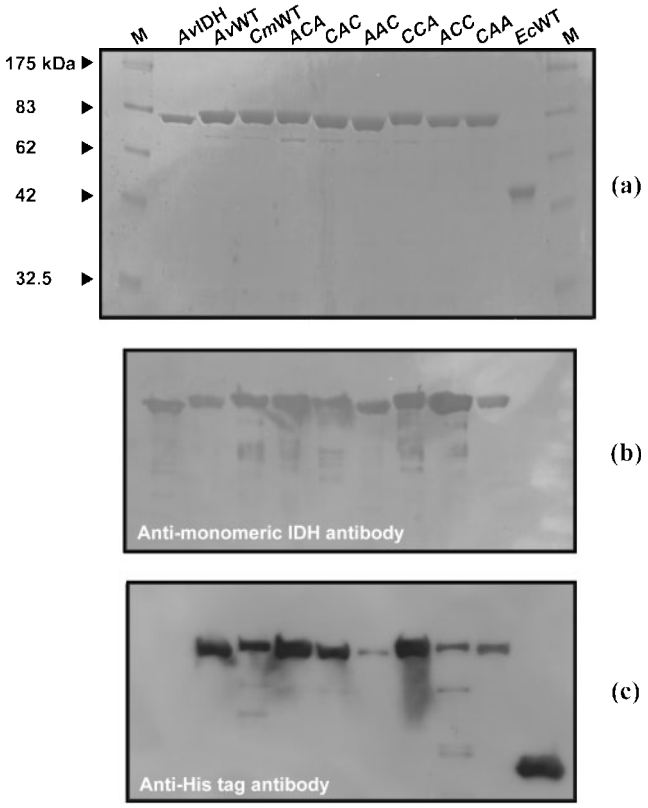

Fig. 2. SDS-PAGE (a) and immunoblot analysis (b, c) of purified wild-type and chimeric IDHs. *Av*IDH indicates the native enzyme protein purified from the *A. vinelandii* cells. M, marker proteins. (a) Five micrograms of each protein was applied. Protein on the gel was stained with Coomassie brilliant blue. (b) and (c) After SDS-PAGE of 2·5 μg protein per lane, antibodies against monomeric IDH of *V. parahaemolyticus* (b) and N-terminal His-tag (c) were used for immunoblotting. Both of the antibodies (20 mg ml^{-1}) were diluted 1 : 2500.

His-tags (47·5 °C and 25 °C, respectively) were analogous to those of the respective native enzymes (40–45 °C and 20 °C, respectively) (Sahara, 2000; Ochiai *et al.*, 1979). All chimeric IDHs exhibited T_{opt} values within the range of those of *Av*WT and *Cm*WT. The T_{opt} of *CAC*, *AAC* and *ACC* (27·5 °C) was only slightly higher than that of *Cm*WT, while the corresponding values of *ACA*, *CCA* and *CAA* (32·5 °C, 32·5–37·5 °C and 42·5 °C, respectively) were higher than those of the former three chimeric IDHs. These results suggest that region 3, located at the C-terminal of *Cm*IDH and *Av*IDH, is involved in determining T_{opt}. The dimeric *Ec*WT exhibited a similar T_{opt} to *Av*WT.

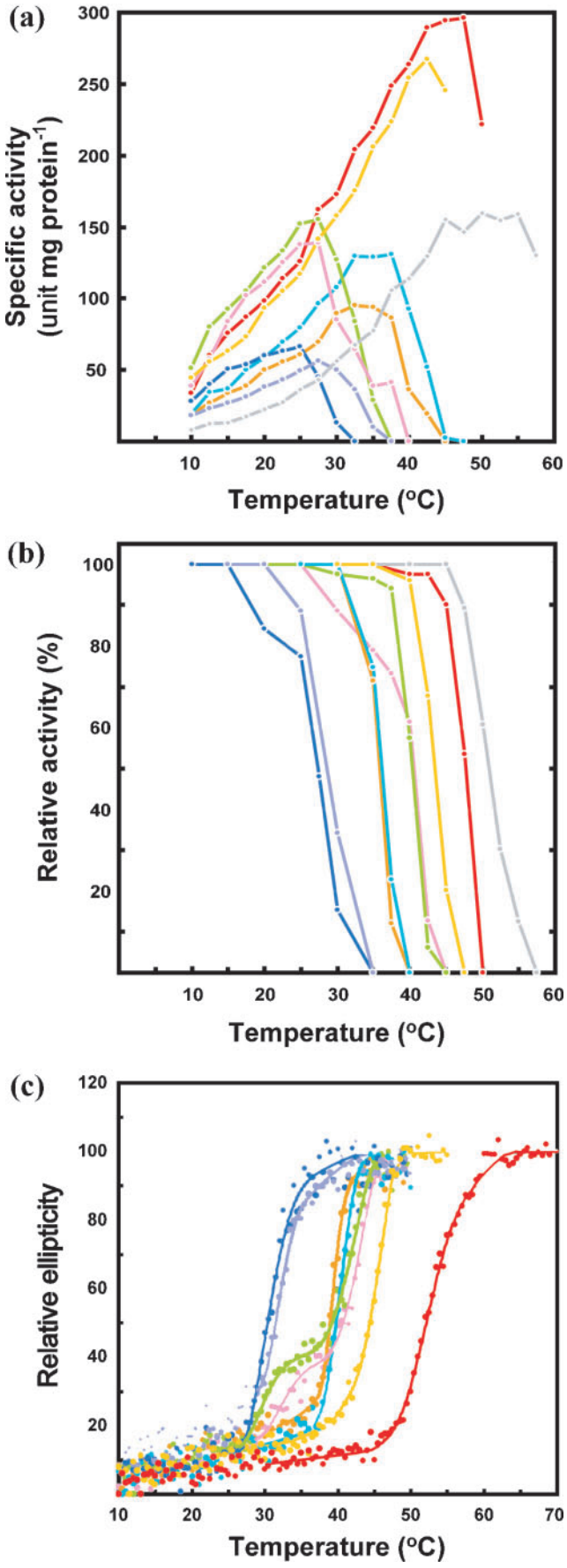

Fig. 3. Effect of temperature on specific activities (a) and thermostability (b, c) of wild-type and chimeric IDHs. Red, *Av*WT; blue, *Cm*WT; light green, *CAC*; orange, *ACA*; pink, *AAC*; sky blue, *CCA*; light blue, *ACC*; yellow, *CAA*; grey, *Ec*WT. (b) Inactivation of enzymes by incubation at various temperatures. (c) Thermal unfolding of the enzyme proteins monitored by CD.

*Av*WT and *Cm*WT exhibited the same thermostability of activity as the respective native enzymes (Ochiai *et al.*, 1979; Sahara, 2000) (Fig. 3b). Furthermore, the thermostability of *Ec*WT activity was similar to that of *Av*WT. Half-lives ($t_{1/2}$) for the heat-inactivation of the chimeric enzymes were intermediate between those of the two wild-types, *Av*WT and *Cm*WT. The thermostability of chimeric IDH activities was fundamentally correlated with the optimal temperatures, that is, chimeric IDHs showing lower optimal temperatures were more thermolabile. However, the $t_{1/2}$ values of *ACA* and *CAC* were 38 °C and 40·5 °C, respectively, and *CAC* was more thermostable than *ACA*, in spite of its lower T_{opt}. Similarly, the T_{opt} of *CCA* was higher than that of *AAC*, but the $t_{1/2}$ values of *CCA* and *AAC* were 37·5 °C and 40·5 °C, respectively.

In addition, the thermostability of the structure of the IDH proteins was monitored by CD (Fig. 3c). The wild-type and chimeric IDHs were classified into two groups based on the thermal denaturation profiles. The first group comprised *Av*WT, *Cm*WT, *ACA*, *CCA*, *ACC* and *CAA* with a monophasic denaturation process. The second was composed of *CAC* and *AAC*, which are denatured in two steps with the presence of a stable intermediate. *ACC* possessed almost the same T_m (temperature at which a half-change in the ellipticity occurred) as *Cm*WT (31·5 °C and 30·5 °C, respectively), whereas the T_m value of *CAA* was closest to that of *Av*WT of all the chimeric IDHs (45 °C and 51 °C, respectively), indicating that the exchange of region 1 had little effect on the thermostability of *Av*WT and *Cm*WT. This possibility was supported by the finding that *ACA* had almost the same denaturation curves and T_m values as *CCA* (39·5 °C and 41 °C, respectively). Conversely, since *ACA* and *CCA* showed T_m values intermediate between those of *Av*WT and *Cm*WT, region 2 of *Av*IDH and region 3 of *Cm*IDH may be determinants of thermostability. On the other hand, T_m values for the first step of denaturation of *CAC* and *AAC* (31 °C and 33 °C, respectively) were similar to the T_m of *Cm*WT. This result suggests that the region(s) derived from *Cm*IDH in these chimeric enzymes are denatured in preference to the one(s) from *Av*IDH. After the incubation above 40 °C, at which the second denaturation step started, the activities of *CAC* and *AAC* could not be recovered (Fig. 3b), indicating an irreversible inactivation. In contrast, only a slight inactivation of *CAC* was observed after incubation at temperatures between 28 °C and 40 °C, at which the first denaturation step proceeded (Fig. 3b, c). These results indicate that domain I of *CAC* is unfolded reversibly between 30 °C and 40 °C. Thus, the exceptional thermostability of *CAC* and *AAC* activities at the moderate temperatures described above (Fig. 3b) may be attributable to the renaturation of the enzymes on cooling after the incubation.

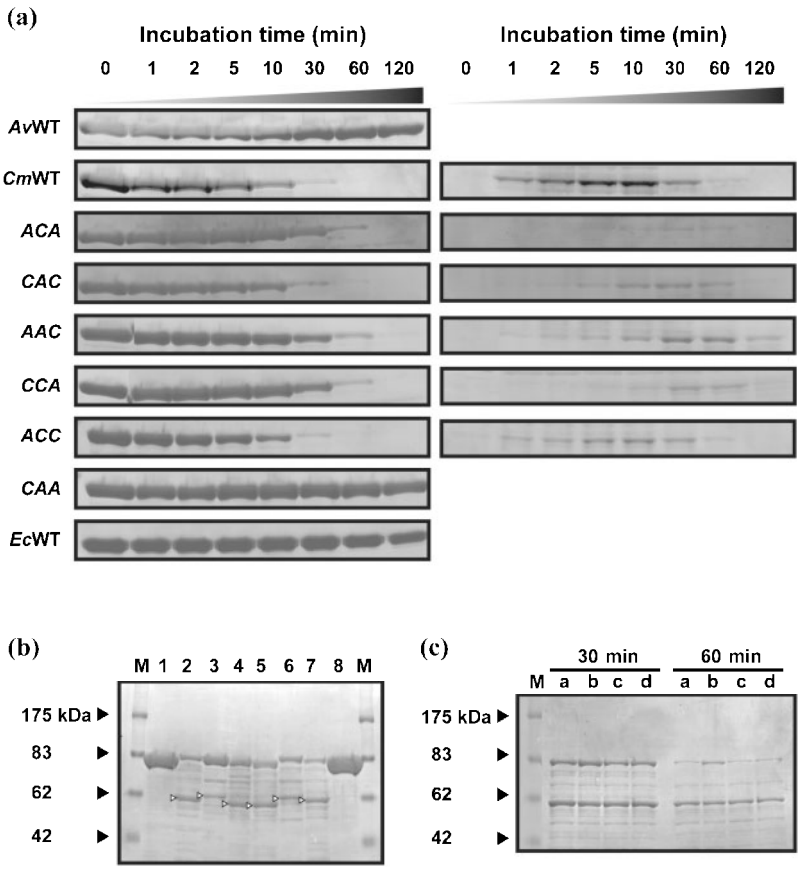

Fig. 4. Digestion of wild-type and chimeric IDHs with trypsin. (a) Time-course of tryptic digestion. The IDH samples were treated for the indicated times with trypsin under the standard conditions described in Methods. Ten micrograms of the enzyme was withdrawn and immediately electrophoresed. After electrophoresis, protein on the gel was stained with Coomassie brilliant blue. Left and right panels indicate the bands of undigested molecules and major digestive intermediates [corresponding to white triangles in (b)], respectively. (b) SDS-PAGE after partial digestion with trypsin. Lane 1, *Av*WT; lane 2, *Cm*WT; lane 3, *ACA*; lane 4, *CAC*; lane 5, *AAC*; lane 6, *CCA*; lane 7, *ACC*; lane 8, *CAA*. All IDH samples (10 μg) were digested for 30 min under standard conditions. White triangles show major digestive intermediates. M, molecular marker proteins. (c) Effect of ligands on the digestion of *Cm*WT with trypsin. *Cm*WT (1 mg ml^{-1}) was incubated for 30 or 60 min at 25 °C with trypsin (0·01 mg ml^{-1}) in the absence (lanes a) or presence of 10 mM isocitrate and 6·7 mM Mn^{2+} (lanes b), 1·2 mM $NADP^+$ (lanes c) or 10 mM isocitrate and 1·2 mM $NADP^+$ (lanes d). The digestion was terminated by the addition of 2× SDS-PAGE sample buffer and subsequent boiling.

Resistance to trypsin

The sensitivity of wild-type and chimeric IDHs to tryptic digestion was examined (Fig. 4a). At 25 °C, *Av*WT and *Ec*WT were little digested after incubation for 120 min with trypsin, while *Cm*WT was rapidly digested with a $t_{½}$ of about 5 min. Six chimeric IDHs were classified into the following three groups based on sensitivity to trypsin: *CAC* and *ACC*, exhibiting a sensitivity to trypsin similar to *Cm*WT; *CAA*, resistant to trypsin in a similar manner to *Av*WT; and *ACA*, *AAC* and *CCA*, with an intermediate level of resistance. The sensitivity of wild-type and chimeric IDHs to tryptic digestion was significantly correlated to the thermostability of their activity and protein structure (Fig. 3b, c). SDS-PAGE of *Cm*WT, *ACA*, *CAC*, *AAC*, *CCA* and *ACC* digested with trypsin (Fig. 4b, lanes 2–7) revealed that the undigested enzyme proteins (83 kDa) and their digestive intermediates (58–62 kDa, white triangles in Fig. 4b) were contained as two major bands, and that the latter accumulated with the decrease of the former. The proteolytic intermediates of chimeric IDHs appeared later than those of *Cm*WT, indicating that the chimeric proteins are more resistant to digestion than *Cm*WT (Fig. 4a, right-hand panel). The apparent molecular masses of the digestive intermediates estimated by SDS-PAGE indicated that none of them are regions 1–3 themselves. N-terminal amino acid sequencing revealed that the intermediates from *CAC* and *AAC* have an N-terminal sequence (KHPHKMGA) corresponding to the sequence from Lys^{157} to Ala^{164} in *Av*IDH. On the other hand, the N-terminal sequence of intermediates from *Cm*WT, *CCA* and *ACC* was found to be NNPHSMGA, which is the homologous sequence from Asn^{159} to Ala^{166} in *Cm*IDH. Because the six IDH enzymes were digested at homologous positions with trypsin, we conclude that the slight differences in the molecular masses of their intermediates were due to different cleavage sites at the C-terminus. By digestion with carboxypeptidase Y, the C-terminal structure of the intermediate from *Cm*WT was identified as EEK, corresponding to the sequence from Glu^{696} to Lys^{698} of *Cm*IDH (Fig. 5b, e). Furthermore, a major value of 58 646·23 Da obtained by MALDI-TOF mass spectrometry was nearly consistent with the theoretical mass of the fragment from Asn^{159} to Lys^{698} of *Cm*IDH (58 663·87 Da). These results indicate that the proteolytic intermediates were produced by the digestion of region 1 and the C-terminal part of region 3 in domain I (Fig. 5b). Although the effects of ligands such as substrate and coenzyme on the tryptic digestion of *Cm*WT were also examined, Mg^{2+}, isocitrate and $NADP^+$, even when more than one of them was added, were not able to protect *Cm*WT from digestion (Fig. 4c).

Comparison between wild-type *Av*WT, *Cm*WT and *Ec*WT and chimeric IDH activity

Both of the monomeric IDHs, *Av*WT and *Cm*WT, exhibited much higher specific activity at low temperatures than the dimeric *Ec*WT (Fig. 3a). A larger difference was observed when the molar catalytic activity (k_{cat}) of the former two IDHs was compared with that of *Ec*WT (Table 1). The affinity for $NADP^+$ of the three IDHs was similar, but the K_m value for isocitrate of *Av*WT was eightfold smaller than that of *Cm*WT and almost the same as that of *Ec*WT. In contrast to *Ec*WT, *Av*WT maintained higher specific and molar catalytic activities even at low temperatures than the cold-adapted *Cm*WT, indicating that *Av*IDH can perform its catalytic function over a wide range of temperatures, in spite of its mesophilic characteristics. Based on the relationship between the stability and activity of the enzyme, the chimeric IDHs could be classified into two groups. *ACA* and *CCA* were more stable, but had lower activity at low temperatures than *Cm*WT. On the other hand, *CAC* and *AAC* had almost the same optimal temperature for activity as *Cm*WT, but the activities of the two chimeric IDHs were enhanced at low temperatures. Furthermore, the K_m values for isocitrate of *ACA*, *CCA* and *CAA* were comparable to that of *Av*WT, indicating that region 3 of *Av*WT is required to increase affinity for this substrate.

DISCUSSION

The cold-adapted monomeric IDH-II from *C. maris* (*Cm*IDH) has been shown to be much more thermolabile than its mesophilic counterpart in *A. vinelandii* (*Av*IDH) (Ochiai *et al.*, 1979; Sahara, 2000), in spite of the similarity in their amino acid sequences (Sahara *et al.*, 2002) and protein structures, as estimated from far-UV CD spectra (data not shown). The three-dimensional structure of *Av*IDH (Yasutake *et al.*, 2002, 2003) consists of three regions (Fig. 1e). Therefore, to specify the structural characteristics responsible for the psychrophilic nature of *Cm*IDH, chimeric IDHs exchanging each region of the two enzymes were constructed and characterized. *CAA* and *ACC* showed characteristics similar to *Av*WT and *Cm*WT, respectively (Fig. 3 and Table 1), indicating that region 1 of the two wild-type IDHs contributes little to their stability and temperature dependence. This region exhibited the highest level of homology in amino acid sequence (74 % identity) among the three regions of *Av*IDH and *Cm*IDH (Sahara *et al.*, 2002). On the other hand, region 2 of *Av*IDH is necessary for the thermostability and high catalytic activity, but not the affinity for isocitrate (Fig. 3 and Table 1). Domain II (region 2) of monomeric IDH consists of two repetitive structural motifs, corresponding to domains B–C from the same two subunits of the dimeric IDH (Fig. 1a–d). A bundle of four helices, formed by two helices from the two motifs, is very hydrophobic in the *Av*IDH and *Cm*IDH proteins, but several hydrophobic amino acid residues of *Av*IDH (Met^{356}, Ile^{357}, Val^{388}, Ile^{390} and Ile^{532}) are replaced by other hydrophobic ones with smaller side-chain volumes in *Cm*IDH (Ala^{354}, Leu^{355}, Ala^{386}, Val^{388} and Val^{530}, respectively). Dimeric isopropylmalate dehydrogenase (IPMDH) has a similar structural framework to the dimeric IDH (Imada *et al.*, 1991). The increased hydrophobicity of the helix bundle in mesophilic IPMDH caused by mutations leads to a strengthened thermostability comparable to that of the thermophilic

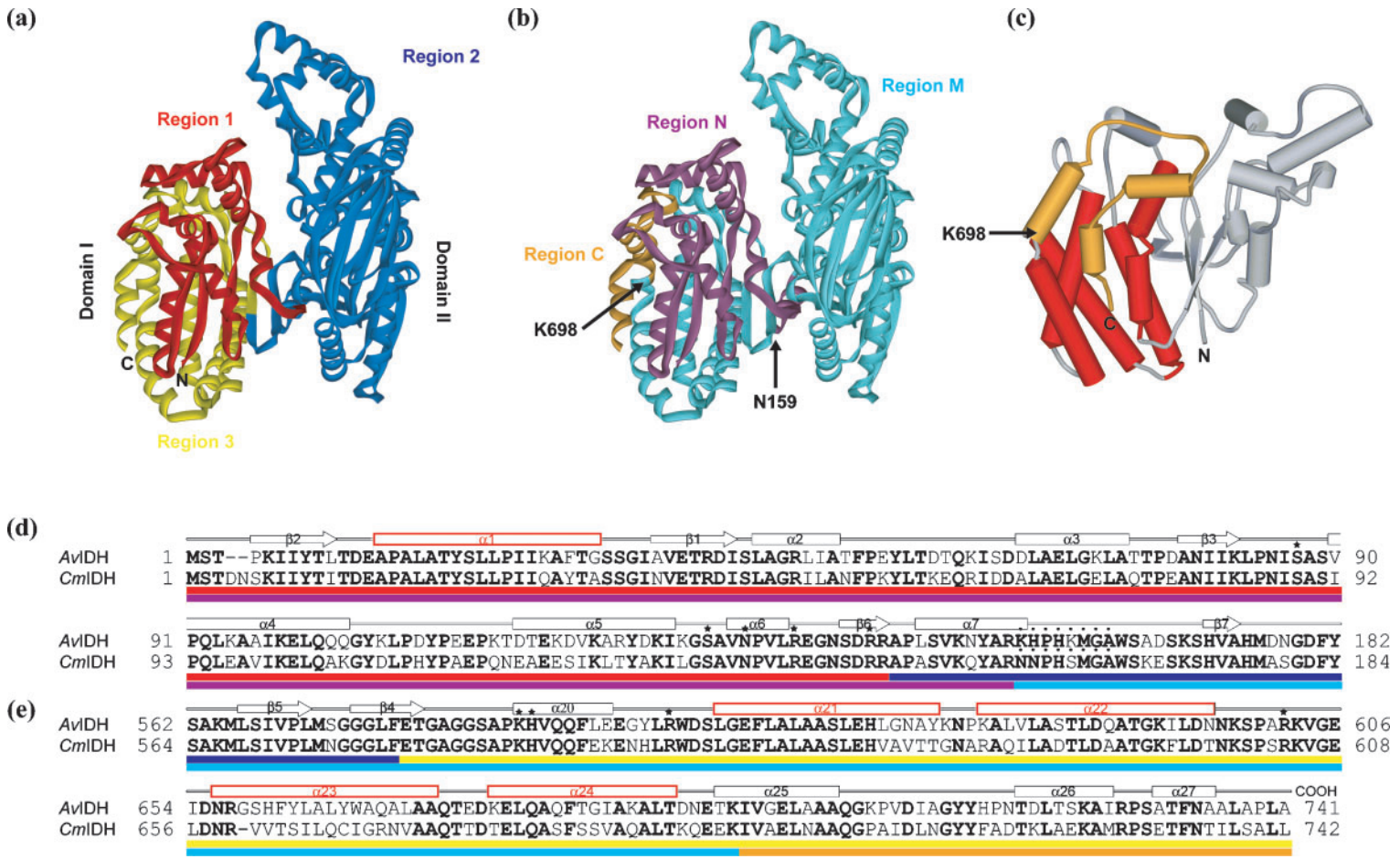

Fig. 5. Major digestive intermediate of *Cm*WT. (a) Ribbon model of monomeric *Av*IDH and its respective regions. Region 1 (Thr[3] to Arg[146], red), region 2 (Ala[147] to Leu[577], blue), region 3 (Phe[578] to Leu[740], yellow). N and C indicate each terminus. (b) Structure of a major digestive intermediate of *Cm*WT. Region M (Asn[159] to Lys[698], light blue) corresponds to the digestive intermediate. (c) Cα trace of domain I of *Cm*WT. The helix bundle consisting of α1 from region 1 and α21–24 from region 3 is shown as red cylinders. The orange region is region C in (b). (d) and (e) Partial amino acid sequence alignments of *Av*IDH and *Cm*IDH. Bold type indicates the amino acid residues conserved between the two enzymes. Stars represent the amino acid residues involved in the catalytic site (see Fig. 1d). Coloured bars under the sequence correspond to the coloured regions in (b). Secondary structures, α-helix (rectangles) and β-sheet (arrows), are shown on the sequence. Red-outlined rectangles are α-helices forming the bundle in domain I represented in (c). Dotted letters are amino acid residues determined by N-terminal sequencing of the digestive intermediates (see text).

Table 1. Kinetic parameters for wild-type and chimeric IDHs at 15 °C

Values shown are the mean of three independent experiments ± SEM.

Enzyme	Standard assay*		Isocitrate†			NADP†		
	Specific activity (μmol min^{-1} mg^{-1})	k_{cat} (s^{-1})	K_m (μM)	k_{cat} (s^{-1})	$k_{cat}/K_m \times 10^5$ (s^{-1} M^{-1})	K_m (μM)	k_{cat} (s^{-1})	$k_{cat}/K_m \times 10^6$ (s^{-1} M^{-1})
*Av*WT	75·5 ± 3·9	105·5 ± 5·5	7·9 ± 0·5	73·0 ± 6·0	92·7	5·8 ± 0·4	92·6 ± 6·1	15·9
*Cm*WT	50·5 ± 1·5	70·8 ± 2·1	62·2 ± 3·2	57·5 ± 0·8	9·2	6·9 ± 0·5	61·3 ± 4·7	9·0
ACA	33·9 ± 2·2	47·4 ± 3·1	11·3 ± 0·4	45·9 ± 2·2	4·0	9·1 ± 0·2	36·8 ± 3·9	4·0
CAC	89·8 ± 2·9	129·9 ± 4·1	93·4 ± 1·3	97·1 ± 4·7	10·4	9·0 ± 0·7	94·3 ± 5·3	10·5
AAC	75·0 ± 9·0	117·4 ± 12·6	154·3 ± 10·3	138·9 ± 17·1	9·0	6·2 ± 0·4	96·2 ± 3·5	15·4
CCA	37·0 ± 0·6	51·9 ± 0·8	8·5 ± 0·8	44·2 ± 5·8	51·9	23·1 ± 0·5	61·3 ± 2·4	2·7
ACC	26·6 ± 0·8	37·2 ± 1·1	28·3 ± 2·2	35·5 ± 4·2	12·5	4·2 ± 0·9	42·7 ± 1·3	10·1
CAA	63·5 ± 0·0	89·3 ± 0·0	12·0 ± 2·5	89·1 ± 7·9	74·6	8·8 ± 0·5	94·3 ± 4·2	10·7
*Ec*WT	13·4 ± 0·3	22·0 ± 0·5‡	3·3 ± 0·1	15·4 ± 1·1‡	4·7‡	7·7 ± 0·1	18·8 ± 0·7‡	2·4‡

*The reaction mixture contained 0·12 mM $NADP^+$ and 2 mM isocitrate, as described in Methods.

†The K_m values for isocitrate and $NADP^+$ were determined by varying the concentrations of isocitrate and $NADP^+$ under standard assay conditions. The data were analysed by Lineweaver–Burk plotting. The following molecular masses of His-tagged recombinant IDHs were used for calculation: *Av*WT (83 898·37 Da, 773 aa), *Cm*WT (84 134·21 Da, 774 aa), *ACA* (83 949·12 Da, 773 aa), *CAC* (84 083·46 Da, 774 aa), *AAC* (83 835·29 Da, 772 aa), *CCA* (84 197·29 Da, 775 aa), *ACC* (83 886·04 Da, 772 aa), *CAA* (84 146·54 Da, 775 aa) and *Ec*WT (98 531·36 Da, 448 aa).

‡k_{cat} values per catalytic site.

counterpart (Kirino *et al.*, 1994; Wallon *et al.*, 1997a). As reported in a psychrophilic IPMDH (Wallon *et al.*, 1997b), larger cavities between helices in the bundle of *Cm*IDH, which are derived from substitution by amino acid residues with smaller side chains, might be responsible for the low stability. The reduced stability of psychrophilic enzymes is considered to give them activation energies lower than those of their mesophilic and thermophilic homologues (Fields, 2001). In fact, the activation energy of *Cm*WT calculated by Arrhenius plotting of the data in Fig. 3a was smaller than that of *Av*WT (8·9 and 17·1 kJ mol^{-1}, respectively).

Region 3 of *Cm*IDH is related to some unique properties of the chimeric enzymes. First, the results of the thermal denaturation of the wild-type and chimeric IDHs and the thermostability of their activities (Fig. 3b, c) indicated that region 3 of *Cm*IDH is responsible for its thermolability and may initially unfold when this enzyme is heat-denatured. Second, the introduction of *Cm*IDH region 3 into the chimeric IDHs led to a reduction of the affinity for isocitrate (*CAC*, *AAC* and *ACC* in Table 1). This can be explained by the general insight for cold-adapted enzymes that their thermolability is attributable to an enhanced structural flexibility compared to their mesophilic and thermophilic counterparts, and that such a flexible structure accompanies a broader distribution of conformational states and results in poor binding to the ligand and high K_m values (Gerday *et al.*, 1997). It has been reported that the high flexibility of cold-adapted lactate dehydrogenases from Antarctic fishes is localized in a limited region involved in catalytic conformational changes, rather than the entire molecule (Fields & Somero, 1998).

Limited proteolysis is useful to clarify the structural configuration of proteins and to identify exposed and flexible regions in the native structure (Aghajanian *et al.*, 2003). The resistance of wild-type and chimeric IDHs to digestion with trypsin is in good agreement with their thermostability (Figs 3 and 4). N-terminal amino acid sequencing and MALDI-TOF mass spectrometric analysis of the intermediates of *Cm*WT and of five chimeric IDHs, not including *CAA*, revealed that trypsin cleavage occurred between Arg^{158} and Asn^{159} and between Lys^{698} and Ile^{699} in the *Cm*IDH sequence, with the resultant generation of the light-blue-coloured fragment (region M) in Fig. 5(b, d, e). Since *CAA* was resistant to trypsin in a similar manner to *Av*WT (Fig. 4a, b), trypsin should digest the C-terminal fragment containing 44 amino acid residues of *Cm*IDH (orange-coloured region C in Fig. 5b, c, e) prior to the N-terminal fragment of 149 amino acid residues (violet-coloured region N). Region C consists of three short α-helices, is located at the surface of the molecule, far from the active-site cleft, and contains no amino acid residue involved in the active site (Fig. 5e), suggesting that the coexistence of ligands such as isocitrate, $NADP^+$ and Mg^{2+} cannot protect the IDH proteins from tryptic digestion. The data in Fig. 4c support this possibility. Therefore, region 3, in particular region C, of *Cm*IDH, responsible for the thermolability, is concluded to be more sensitive to tryptic digestion than the other regions. Domain I of monomeric IDH contains many α-helices, and four helices in region 3, α21–α24, form a helix bundle together with α1 in region 1 (red cylinders in Fig. 5c). In contrast to these tight interactions, region C, located on the surface, should be flexible, since Pro^{709}, Pro^{718} and Pro^{739} in this region of *Av*IDH possess much

higher *B* factors than the mean for the whole molecule (data not shown). Therefore, region C of *Cm*IDH might be more flexible than that of *Av*IDH. On the other hand, *Cm*IDH has a smaller number and content of Pro residues than *Av*IDH (the former, 31 and 4·2 %; the latter, 37 and 5·0 %). This has been proposed to be a general characteristic of cold-adapted enzymes (Gerday *et al.*, 1997; Wallon *et al.*, 1997b). Notably, a Pro residue in a loop region diminishes the flexibility of the main chains of the protein as well as the entropy of unfolding, since the pyrrolidine ring severely restricts possible conformations of the preceding residue (Matthews *et al.*, 1987). In short loops in region C, the Pro^{718} and Pro^{739} of *Av*IDH are substituted for Ala^{719} and Ala^{740}, respectively, in *Cm*IDH (Fig. 5e). Furthermore, the replacement of His^{717} of *Av*IDH with Phe in *Cm*IDH may weaken the stability of region C in the latter enzyme, because the His residue forms a hydrogen bond with Tyr^{105} of region N in *Av*IDH, but the His residue is lost in *Cm*IDH, in spite of the conservation of the Tyr residue (Tyr^{107} in *Cm*IDH).

$NADP^+$-IDH is a member of the β-decarboxylating dehydrogenase family, which catalyses metal ion- and $NAD(P)^+$-dependent dehydrogenation and subsequent metal ion-dependent decarboxylation of 2*R*,3*S*-2-hydroxy acids. NAD^+-IDH, NAD^+-IPMDH, NAD^+-homo-isocitrate dehydrogenase (HDH) and NAD^+-tartrate dehydrogenase (TDH) are contained in this family (Chen & Jeong, 2000). Among them, all IPMDHs, HDHs and TDHs, and most IDHs, are dimers. From phylogenetic analyses and comparisons of the crystal structures of $NADP^+$-*Ec*IDH, pig mitochondrial and human cytosolic dimeric $NADP^+$-IDHs and dimeric NAD^+-IPMDH of *Thermus thermophilus*, it has been proposed that the ancestor had to be a dimeric enzyme with a broad specificity for substrates and coenzymes (Hurley *et al.*, 1989, 1991; Imada *et al.*, 1991; Dean & Golding, 1997; Steen *et al.*, 2001; Stoddard *et al.*, 1993; Ceccarelli *et al.*, 2002; Xu *et al.*, 2004; Hurley & Dean, 1994). On the other hand, the structure of monomeric *Av*IDH (Fig. 1) suggests that the monomeric IDHs did not evolve convergently but originated from the common ancestor for this enzyme family by a unique domain duplication (Yasutake *et al.*, 2002). The specific activities of monomeric *Av*IDH and *Cm*IDH at 15 °C were higher than that of dimeric *Ec*IDH (5·6- and 3·8-fold, respectively; Table 1). Furthermore, at all temperatures tested, *Av*IDH showed higher activities than *Ec*IDH (Fig. 3a). Similar results have been reported for other monomeric IDHs from mesophilic bacteria (Chen & Yang, 2000; Kanao *et al.*, 2002). At 15 °C, the K_m values for isocitrate and $NADP^+$ of *Av*IDH were almost the same as those of *Ec*IDH, but the catalytic efficiency (k_{cat}/K_m) of the former was 20-fold higher than that of the latter (Table 1). Similarly, at 37 °C, the K_m for isocitrate and $NADP^+$ and k_{cat}/K_m of the two IDHs has been reported to be 36 and 23 μM and $3{\cdot}1 \times 10^9$ s^{-1} M^{-1} for *Av*IDH and 17 and 11 μM and $7{\cdot}3 \times 10^6$ s^{-1} M^{-1} for *Ec*IDH, respectively (Barrera & Jurtshuk, 1970; Chen & Yang, 2000). This implies that the monomeric IDHs cope with the loss of a catalytic site due to the monomerization through improving the catalytic rates. The amino acid residues involved in the binding to isocitrate and Mn^{2+} (or Mg^{2+}) are conserved between *Av*IDH and *Ec*IDH (Fig. 1c, d). *Ec*IDH is bound to $NADP^+$ by hydrogen bonds between the 2′-phosphate of $NADP^+$ and some of the amino acid residues and by electrostatic attractions to the charged isocitrate–Mg^{2+} complex as the true substrate (Hurley *et al.*, 1991; Stoddard *et al.*, 1993). Moreover, *Av*IDH can form an additional hydrogen bond between the nicotinamide ring of the bound $NADP^+$ and the side chain of Ser^{87} (Fig. 1d) (Yasutake *et al.*, 2003), implying that the resultant stabilized Michaelis ES complex leads to a rapid conversion to reaction products. The similar K_m values for $NADP^+$ of *Av*IDH and *Ec*IDH (Table 1) suggest that the catalysis of *Av*IDH is due to the random binding mechanism between ligand(s), as reported for *Ec*IDH (Stoddard *et al.*, 1993).

It is noteworthy that *Av*IDH exhibited higher specific activity at low temperatures than mesophilic *Ec*IDH and even than cold-adapted *Cm*IDH (Fig. 3a). Nevertheless, this enzyme does not possess the unique characteristics in amino acid sequence and structure which have been reported in cold-adapted and/or -active enzymes, such as lower numbers of several hydrophobic and/or charged amino acid residues than their mesophilic and thermophilic counterparts (Gerday *et al.*, 1997; Russell *et al.*, 1998; Bentahir *et al.*, 2000), extension of the surface loop and optimization of the surface potentials (Kim *et al.*, 1999; de Backer *et al.*, 2002), which are responsible for the weakened intermolecular interactions, and increased structural flexibility. In fact, *Av*IDH shows typical mesophilic thermostability and the same resistance to trypsin as *Ec*IDH (Figs 3 and 4). Similar results were reported for a mutant, 3-2G7, of the cold-adapted subtilisin S41 from Antarctic *Bacillus* TA41 which retains psychrophilic characteristics and acquires markedly increased thermostability (Miyazaki *et al.*, 2000). The existence of such enzymes, including *Av*IDH, indicates that the thermolability of the enzyme proteins is not always essential for high catalytic activity under cold conditions. Thus, further detailed studies of *Av*IDH, of which the three-dimensional structure has been resolved, should provide valuable information for solving this problem. On the other hand, *in vivo* transcription of the *Cm*IDH gene is induced by low temperature, and the growth of the *E. coli icd*-defective mutant at low temperatures is improved by the transformation of a plasmid carrying the gene encoding *Cm*IDH (Suzuki *et al.*, 1995; Sahara *et al.*, 1999). Furthermore, isocitrate lyase of *C. maris*, which catalyses the cleavage of isocitrate to glyoxylate and succinate, is markedly thermolabile, and the expression of the gene encoding the enzyme is also cold-inducible (Watanabe *et al.*, 2001, 2002). Such a cold-inducible expression of genes for cold-adapted metabolic enzymes seems to be one strategy for adaptation to cold environments. In *C. maris*, the lower catalytic activity of *Cm*IDH at low temperatures than that of *Av*IDH might be

partially compensated by this cold-inducible transcriptional mechanism. These lines of study are in progress in our laboratory.

ACKNOWLEDGEMENTS

We thank Professor Norio Nishi, Division of Bioscience, Graduate School of Environmental Earth Science, Hokkaido University, and Mr Yu-kichi Abe, Center for Instrumental Analysis, Hokkaido University, for kindly lending a spectropolarimeter and for advice on the determination of N- and C-terminal amino acid sequences, respectively.

REFERENCES

Aghajanian, S., Hovsepyan, M., Geoghegan, K. F., Chrunyk, B. A. & Engel, P. C. (2003). A thermally sensitive loop in clostridial glutamate dehydrogenase detected by limited proteolysis. *J Biol Chem* **278**, 1067–1074.

Alvarez, M., Zeelen, J. P., Mainfroid, V., Rentier-Delrue, F., Martial, J. A., Wyns, L., Wierenga, R. K. & Maes, D. (1998). Triose-phosphate isomerase (TIM) of the psychrophilic bacterium *Vibrio marinus*. Kinetic and structural properties. *J Biol Chem* **273**, 2199–2206.

Barrera, C. R. & Jurtshuk, P. (1970). Characterization of the highly active isocitrate ($NADP^+$) dehydrogenase of *Azotobacter vinelandii*. *Biochim Biophys Acta* **220**, 416–429.

Bentahir, M., Feller, G., Aittaleb, M., Lamotte-Brasseur, J., Himri, T., Chessa, J. P. & Gerday, C. (2000). Structural, kinetic, and calorimetric characterization of the cold-active phosphoglycerate kinase from the Antarctic *Pseudomonas* sp. TACII18. *J Biol Chem* **275**, 11147–11153.

Ceccarelli, C., Grodsky, N. B., Ariyaratne, N., Colman, R. F. & Bahnson, B. J. (2002). Crystal structure of porcine mitochondrial $NADP^+$-dependent isocitrate dehydrogenase complexed with Mn^{2+} and isocitrate: insights into the enzyme mechanism. *J Biol Chem* **277**, 43454–43462.

Chen, R. & Jeong, S. S. (2000). Functional prediction: identification of protein orthologs and paralogs. *Protein Sci* **9**, 2344–2353.

Chen, R. & Yang, H. (2000). A highly specific monomeric isocitrate dehydrogenase from *Corynebacterium glutamicum*. *Arch Biochem Biophys* **383**, 238–245.

Dean, A. M. & Golding, G. B. (1997). Protein engineering reveals ancient adaptive replacements in isocitrate dehydrogenase. *Proc Natl Acad Sci U S A* **94**, 3104–3109.

de Backer, M., McSweeney, S., Rasmussen, H. B., Riise, B. W., Lindley, P. & Hough, E. (2002). The 1·9 Å crystal structure of heat-labile shrimp alkaline phosphatase. *J Mol Biol* **318**, 1265–1274.

Eikmanns, B. J., Rittmann, D. & Sahm, H. (1995). Cloning, sequence analysis, expression, and inactivation of the *Corynebacterium glutamicum icd* gene encoding isocitrate dehydrogenase and biochemical characterization of the enzyme. *J Bacteriol* **177**, 774–782.

Fields, P. A. (2001). Protein function at thermal extremes: balancing stability and flexibility. *Comp Biochem Physiol* **A129**, 417–431.

Fields, P. A. & Somero, G. N. (1998). Hot spots in cold adaptation: localized increases in conformational flexibility in lactate dehydrogenase A4 orthologs of antarctic notothenioid fishes. *Proc Natl Acad Sci U S A* **95**, 11476–11481.

Fukunaga, N., Imagawa, S., Sahara, T., Ishii, A. & Suzuki, M. (1992). Purification and characterization of monomeric isocitrate dehydrogenase with $NADP^+$-specificity from *Vibrio parahaemolyticus* Y-4. *J Biochem* **112**, 849–855.

Gerday, C., Aittaleb, M., Arpigny, J. L., Baise, E., Chessa, J. P., Garsoux, G., Petrescu, I. & Feller, G. (1997). Psychrophilic enzymes: a thermodynamic challenge. *Biochim Biophys Acta* **1342**, 119–131.

Hurley, J. H. & Dean, A. M. (1994). Structure of 3-isopropylmalate dehydrogenase in complex with NAD^+: ligand-induced loop closing and mechanism for cofactor specificity. *Structure* **2**, 1007–1016.

Hurley, J. H., Thorsness, P. E., Ramalingam, V., Helmers, N. H., Koshland, D. E., Jr & Stroud, R. M. (1989). Structure of a bacterial enzyme regulated by phosphorylation, isocitrate dehydrogenase. *Proc Natl Acad Sci U S A* **86**, 8635–8639.

Hurley, J. H., Dean, A. M., Koshland, D. E., Jr & Stroud, R. M. (1991). Catalytic mechanism of $NADP^+$-dependent isocitrate dehydrogenase: implications from the structures of magnesium-isocitrate and $NADP^+$ complexes. *Biochemistry* **30**, 8671–8678.

Imada, K., Sato, M., Tanaka, N., Katsube, Y., Matsuura, Y. & Oshima, T. (1991). Three-dimensional structure of a highly thermostable enzyme, 3-isopropylmalate dehydrogenase of *Thermus thermophilus* at 2·2 Å resolution. *J Mol Biol* **222**, 725–738.

Ishii, A., Ochiai, T., Imagawa, S., Fukunaga, N., Sasaki, S., Minowa, O., Mizuno, Y. & Shiokawa, H. (1987). Isozymes of isocitrate dehydrogenase from an obligately psychrophilic bacterium, *Vibrio* sp. strain ABE-1: purification, and modulation of activities by growth conditions. *J Biochem* **102**, 1489–1498.

Ishii, A., Suzuki, M., Sahara, T., Takada, Y., Sasaki, S. & Fukunaga, N. (1993). Genes encoding two isocitrate dehydrogenase isozymes of a psychrophilic bacterium, *Vibrio* sp. strain ABE-1. *J Bacteriol* **175**, 6873–6880.

Kanao, T., Kawamura, M., Fukui, T., Atomi, H. & Imanaka, T. (2002). Characterization of isocitrate dehydrogenase from the green sulfur bacterium *Chlorobium limicola*: a carbon dioxide-fixing enzyme in the reductive tricarboxylic acid cycle. *Eur J Biochem* **269**, 1926–1931.

Kim, S. Y., Hwang, K. Y., Kim, S. H., Sung, H. C., Han, Y. S. & Cho, Y. (1999). Structural basis for cold adaptation. Sequence, biochemical properties, and crystal structure of malate dehydrogenase from a psychrophile *Aquaspirillium arcticum*. *J Biol Chem* **274**, 11761–11767.

Kirino, H., Aoki, M., Aoshima, M., Hayashi, Y., Ohba, M., Yamagishi, A., Wakagi, T. & Oshima, T. (1994). Hydrophobic interaction at the subunit interface contributes to the thermostability of 3-isopropylmalate dehydrogenase from an extreme thermophile, *Thermus thermophilus*. *Eur J Biochem* **220**, 275–281.

Laemmli, U. K. (1970). Cleavage of structural proteins during the assembly of the head of bacteriophage T4. *Nature* **227**, 680–685.

LaPorte, D. C., Thorsness, P. E. & Koshland, D. E., Jr (1985). Compensatory phosphorylation of isocitrate dehydrogenase: a mechanism for adaptation to the intracellular environment. *J Biol Chem* **260**, 10563–10568.

Lowry, O. H., Rosebrough, N. J., Farr, A. L. & Randall, R. J. (1951). Protein measurement with the Folin phenol reagent. *J Biol Chem* **193**, 265–275.

Matthews, B. W., Nicholson, H. & Becktel, W. J. (1987). Enhanced protein thermostability from site-directed mutations that decrease the entropy of unfolding. *Proc Natl Acad Sci U S A* **84**, 6663–6667.

Miyazaki, K., Wintrode, P. L., Grayling, R. A., Rubingh, D. N. & Arnold, F. H. (2000). Directed evolution study of temperature adaptation in a psychrophilic enzyme. *J Mol Biol* **297**, 1015–1026.

Ochiai, T., Fukunaga, N. & Sasaki, S. (1979). Purification and some properties of two $NADP^+$-specific isocitrate dehydrogenases from an obligately psychrophilic marine bacterium, *Vibrio* sp., strain ABE-1. *J Biochem* **86**, 377–384.

Russell, R. J. M., Gerike, U., Danson, M. J., Hough, D. W. & Taylor, G. L. (1998). Structural adaptations of the cold-active citrate synthase from an Antarctic bacterium. *Structure* **6**, 351–361.

Sahara, T. (2000). *Studies on structure and function of the bacterial monomeric isocitrate dehydrogenase and regulatory mechanisms of the gene expression*. Doctoral dissertation, Hokkaido University, Sapporo, Japan.

Sahara, T., Suzuki, M., Tsuruha, J., Takada, Y. & Fukunaga, N. (1999). *cis*-Acting elements responsible for low-temperature-inducible expression of the gene coding for the thermolabile isocitrate dehydrogenase isozyme of a psychrophilic bacterium, *Vibrio* sp. strain ABE-1. *J Bacteriol* **181**, 2602–2611.

Sahara, T., Takada, Y., Takeuchi, Y., Yamaoka, N. & Fukunaga, N. (2002). Cloning, sequencing, and expression of a gene encoding the monomeric isocitrate dehydrogenase of the nitrogen fixing bacterium, *Azotobacter vinelandii*. *Biosci Biotechnol Biochem* **66**, 489–500.

Steen, I. H., Madern, D., Karlstrom, M., Lien, T., Ladenstein, R. & Birkeland, N. K. (2001). Comparison of isocitrate dehydrogenase from three hyperthermophiles reveals differences in thermostability, cofactor specificity, oligomeric state, and phylogenetic affiliation. *J Biol Chem* **276**, 43924–43931.

Stoddard, B. L., Dean, A. & Koshland, D. E., Jr (1993). Structure of isocitrate dehydrogenase with isocitrate, nicotinamide adenine dinucleotide phosphate, and calcium at 2·5-Å resolution: a pseudo-Michaelis ternary complex. *Biochemistry* **32**, 9310–9316.

Suzuki, M., Sahara, T., Tsuruha, J., Takada, Y. & Fukunaga, N. (1995). Differential expression in *Escherichia coli* of the *Vibrio* sp. strain ABE-1 *icd-I* and *icd-II* genes encoding structurally different isocitrate dehydrogenase isozymes. *J Bacteriol* **177**, 2138–2142.

Takada, Y., Ochiai, T., Okuyama, H., Nishi, K. & Sasaki, S. (1979). An obligately psychrophilic bacterium isolated on the Hokkaido coast. *J Gen Appl Microbiol* **25**, 11–19.

Thorsness, P. E. & Koshland, D. E., Jr (1987). Inactivation of isocitrate dehydrogenase by phosphorylation is mediated by the negative charge of the phosphate. *J Biol Chem* **262**, 10422–10425.

Wallon, G., Kryger, G., Lovett, S. T., Oshima, T., Ringe, D. & Petsko, G. A. (1997a). Crystal structures of *Escherichia coli* and *Salmonella typhimurium* 3-isopropylmalate dehydrogenase and comparison with their thermophilic counterpart from *Thermus thermophilus*. *J Mol Biol* **266**, 1016–1031.

Wallon, G., Lovett, S. T., Magyar, C., Svingor, A., Szilagyi, A., Zavodszky, P., Ringe, D. & Petsko, G. A. (1997b). Sequence and homology model of 3-isopropylmalate dehydrogenase from the psychrotrophic bacterium *Vibrio* sp. I5 suggest reasons for thermal instability. *Protein Eng* **10**, 665–672.

Watanabe, S., Takada, Y. & Fukunaga, N. (2001). Purification and characterization of a cold-adapted isocitrate lyase and a malate synthase from *Colwellia maris*, a psychrophilic bacterium. *Biosci Biotechnol Biochem* **65**, 1095–1103.

Watanabe, S., Yamaoka, N., Takada, Y. & Fukunaga, N. (2002). The cold-inducible *icl* gene encoding thermolabile isocitrate lyase of a psychrophilic bacterium, *Colwellia maris*. *Microbiology* **148**, 2579–2589.

Xu, X., Zhao, J., Xu, Z., Peng, B., Huang, Q., Arnold, E. & Ding, J. (2004). Structures of human cytosolic NADP-dependent isocitrate dehydrogenase reveal a novel self-regulatory mechanism of activity. *J Biol Chem* **279**, 33946–33957.

Yasutake, Y., Watanabe, S., Yao, M., Takada, Y., Fukunaga, N. & Tanaka, I. (2001). Crystallization and preliminary X-ray diffraction studies of monomeric isocitrate dehydrogenase by the MAD method using Mn atoms. *Acta Cryst* **D57**, 1682–1685.

Yasutake, Y., Watanabe, S., Yao, M., Takada, Y., Fukunaga, N. & Tanaka, I. (2002). Structure of the monomeric isocitrate dehydrogenase: evidence of a protein monomerization by a domain duplication. *Structure* **10**, 1637–1648.

Yasutake, Y., Watanabe, S., Yao, M., Takada, Y., Fukunaga, N. & Tanaka, I. (2003). Crystal structure of the monomeric isocitrate dehydrogenase in the presence of $NADP^+$: insight into the cofactor recognition, catalysis, and evolution. *J Biol Chem* **278**, 36897–36904.

Yumoto, I., Kawasaki, K., Iwata, H., Matsuyama, H. & Okuyama, H. (1998). Assignment of *Vibrio* sp. strain ABE-1 to *Colwellia maris* sp. nov., a new psychrophilic bacterium. *Int J Syst Bacteriol* **48**, 1357–1362.